

Electronic Supporting Information

Deep-Blue Narrow-Band Emissive Cesium Europium Bromide Perovskite

Nanocrystals with Record High Emission Efficiency for Wide-Color-Gamut Backlight

Displays

Xu Li,^{a,†} Bibo Lou,^{b,†} Xu Chen,^{a*} Meng Wang,^a Huifang Jiang,^a Shuailing Lin,^a Zhuangzhuang Ma,^a Mochen Jia,^a Yanbing Han,^a Yongtao Tian,^a Di Wu,^a Wen Xu,^c Xinjian Li,^a Chonggeng Ma^b and Zhifeng Shi^{a*}

^aKey Laboratory of Material Physics, Ministry of Education, School of Physics and Microelectronics, Zhengzhou University, Zhengzhou 450052, China.

^b School of Optoelectronic Engineering & CQUPT-BUL Innovation Institute, Chongqing University of Posts and Telecommunications, Chongqing 400065, P.R. China.

^cKey Laboratory of New Energy and Rare Earth Resource Utilization of State Ethnic Affairs Commission, School of Physics and Materials Engineering, Dalian Minzu University, Dalian 116600, China.

[†]These authors contributed equally: X.L. and B.L.

*Corresponding author. E-mail: shizf@zzu.edu.cn; xchen@zzu.edu.cn

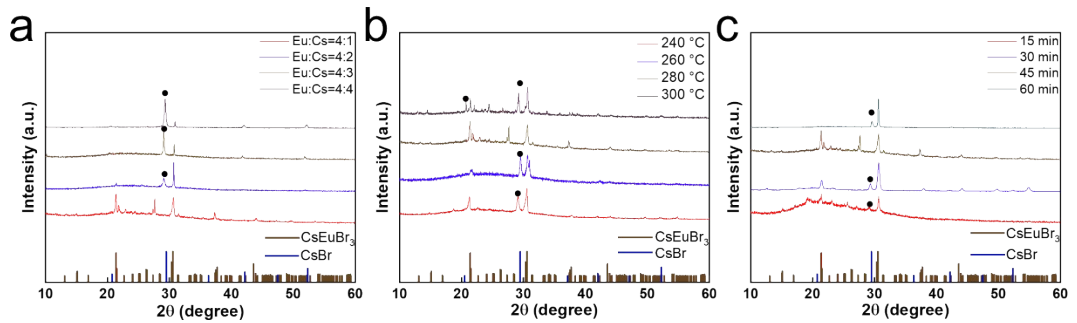


Fig. S1 XRD results of CsEuBr₃ NCs synthesized under different conditions: (a) Addition ratio of Eu/Cs (45 min at 280 °C). (b) The reaction temperature for 45 min reaction time (Eu/Cs=4:1). (c) Reaction time at 280 °C (Eu/Cs=4:1).

In order to explore the synthesis conditions for obtaining pure phase CsEuBr₃ NCs, we characterized CsEuBr₃ NCs synthesized under different conditions using XRD. The results showed that the ratio of Eu/Cs was 4:1, and the XRD was pure phase after reacting at 280 °C for 45 min.

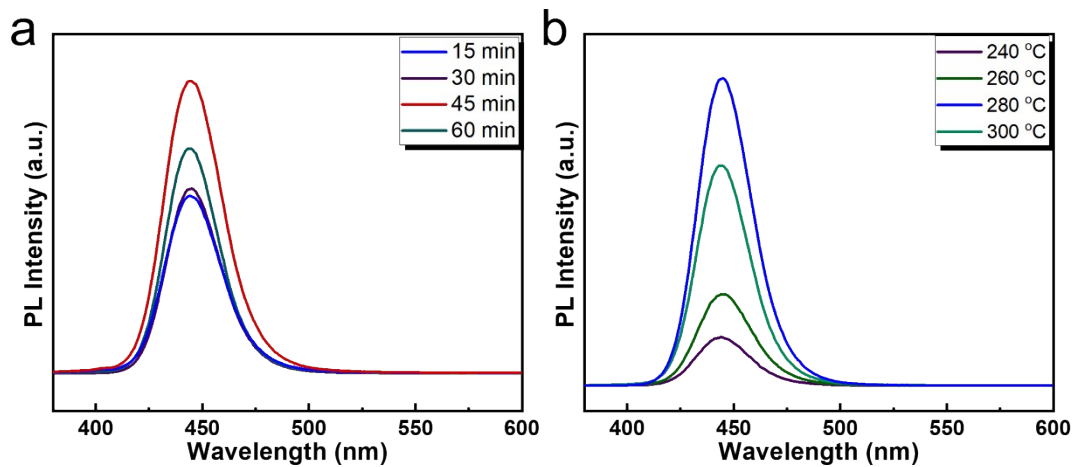


Fig. S2 (a) PL for different reaction time. (b) PL at the different reaction temperatures.

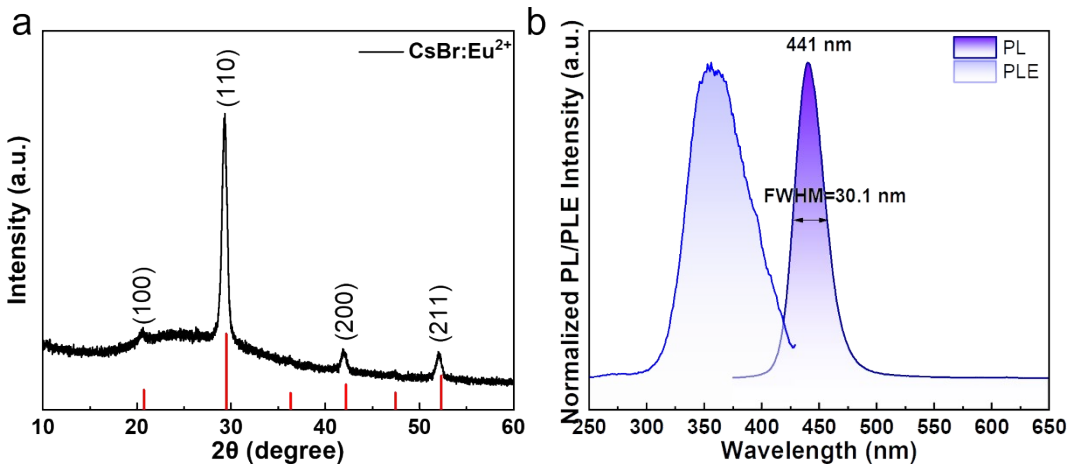


Fig. S3 (a) XRD, (b) PL and PLE of CsBr:Eu²⁺ NCs.

The XRD pattern of CsBr:Eu²⁺ NCs in Fig. S3a is consistent with the standard cards of CsBr (PDF# 061-071-495), and the PL spectrum of CsBr:Eu²⁺ NCs with an emission peak at 441 nm in Fig. S3b.

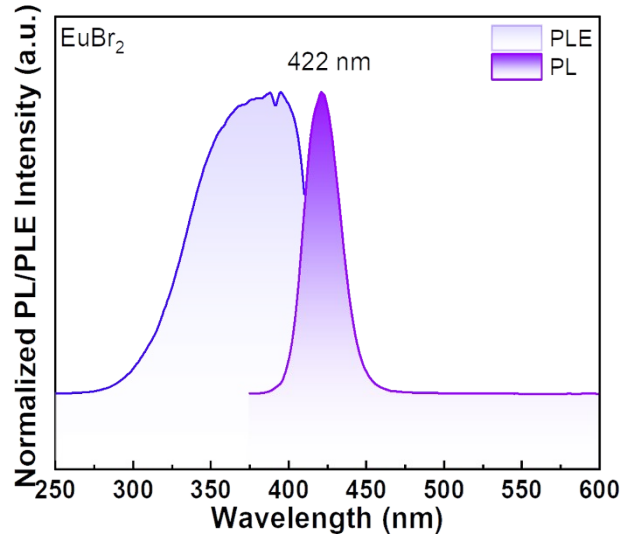


Fig. S4 PL and PLE of EuBr_2 .

The huge difference between EuBr_2 and CsEuBr_3 NCs can rule out the influence of
 EuBr_2 on luminescence.

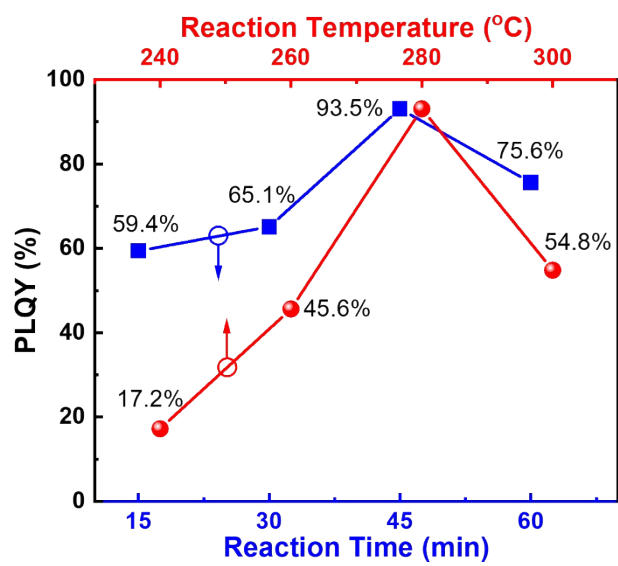


Fig. S5 PLQY variation of CsEuBr_3 NCs synthesized with varying conditions of the reaction

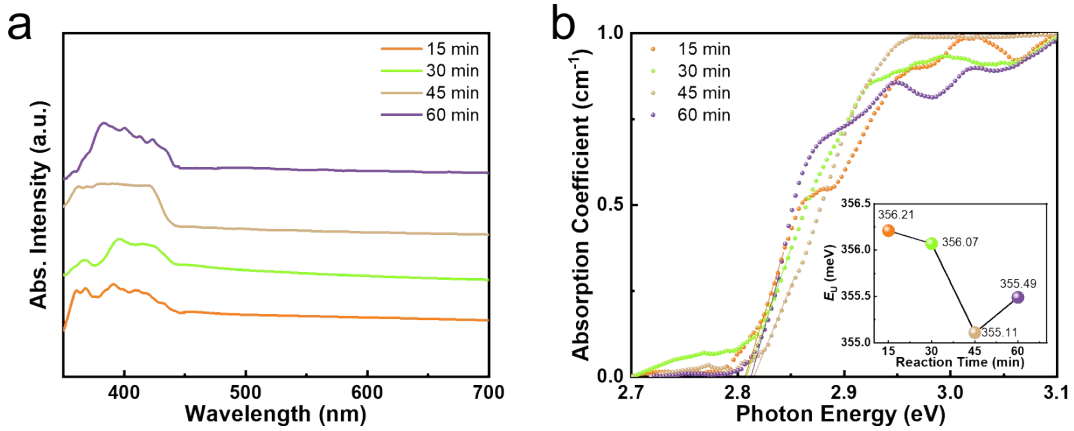


Fig. S6 (a) UV-vis absorption spectra of the NCs prepared at 280 °C with various reaction times. (b) decay of CsEuBr₃ NCs for different reaction times. (c) Urbach energies in different reaction time.

The change in the Urbach energies (E_U) is related to the change in defect density. The larger the E_U , the larger the density of defect states. According to the formula,

$$\alpha(E) = \alpha_0 \exp\left[-\sigma(T) \frac{E - E_0}{k_B T} \right] \quad \text{* MERGEFORMAT (1)}$$

where $\alpha(E)$ is the absorption coefficient as a function of photon energy E , E_0 , and α_0 are the characteristic parameters of the material, $\sigma(T)$ is the steepness factor, k_B is the Boltzmann constant, and T is the absolute temperature. The E_U is defined as $E_U = k_B T / \sigma(T)$. When the reaction time increases from 15 min to 45 min, E_U decreases from 356.21 to 355.11 meV. When the reaction time further increases to 60 min, E_U decreases to 355.49 meV. When the reaction time is 45 min, the corresponding E_U of CsEuBr₃ NCs is the smallest, indicating that the defects are the least at this time. The results are consistent with the PL, PLQY, and TRPL characterization. The results show that as the reaction time increases, the electron disorder and defect density in the NCs will increase, and the optimal reaction time is beneficial for reducing the defect density of CsEuBr₃ NCs.

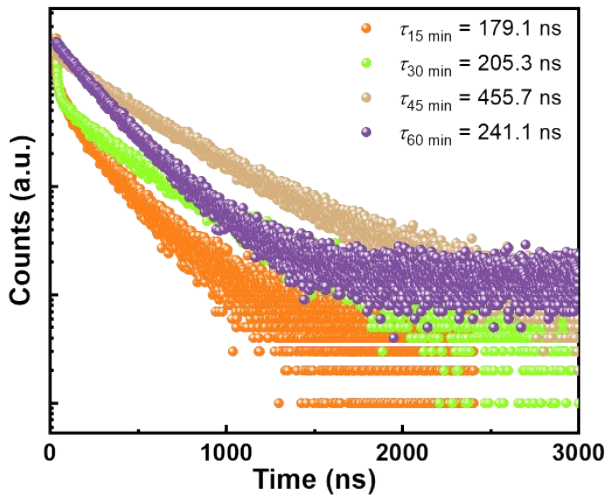


Fig. S7 TRPL of CsEuBr_3 NCs for different reaction times.

The TRPL curve was fitted using a double exponential decay curve:

$$y = A_1 \exp(-t / \tau_1) + A_2 \exp(-t / \tau_2) + I_0 \quad \text{* MERGEFORMAT (2)}$$

$$\tau_{\text{ave}} = \frac{A_1 \tau_1^2 + A_2 \tau_2^2}{A_1 \tau_1 + A_2 \tau_2} \quad \text{* MERGEFORMAT (3)}$$

where τ_1 and τ_2 represent the fast and slow decay processes, associated with the lifetimes of de-trapping to defect states and radiative recombination, respectively. A_1 , A_2 , and I_0 are constants. τ_{ave} represents the average PL lifetime.

As the reaction time increases, the TRPL exhibits a trend of first increasing and then decreasing. τ_{ave} was fitted using eq 2, and the results show that τ_{ave} increases from 179.1 ns to 455.7 ns, indicating that CsEuBr_3 NCs at this reaction temperature have the lowest defect density. When the reaction time increases to 60 min, more organic ligands are replaced on the surface of NCs, resulting in the loss of a certain length of organic ligands as spacing. This promotes their fusion and defect density increase, leading to a loss of good photoelectronic performance.

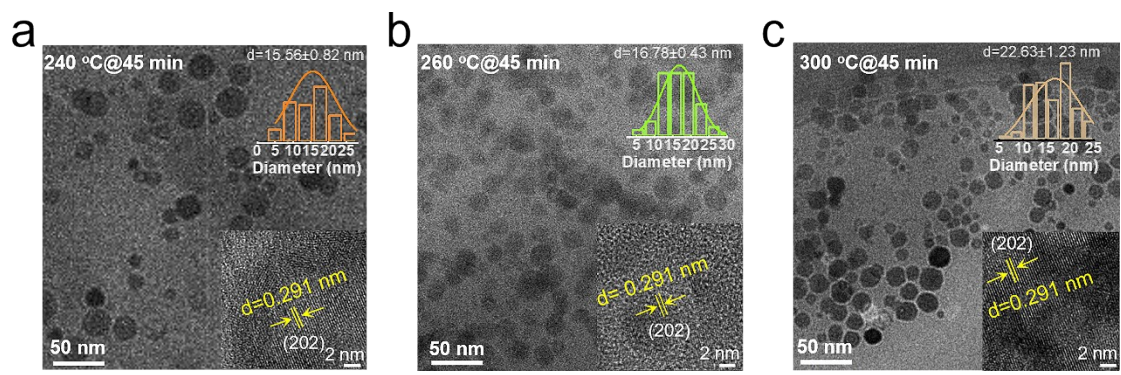


Fig. S8 TEM images of CsEuBr_3 NCs synthesized by reaction at different temperatures:

(a) 240 °C; (b) 260 °C; (c) 300 °C.

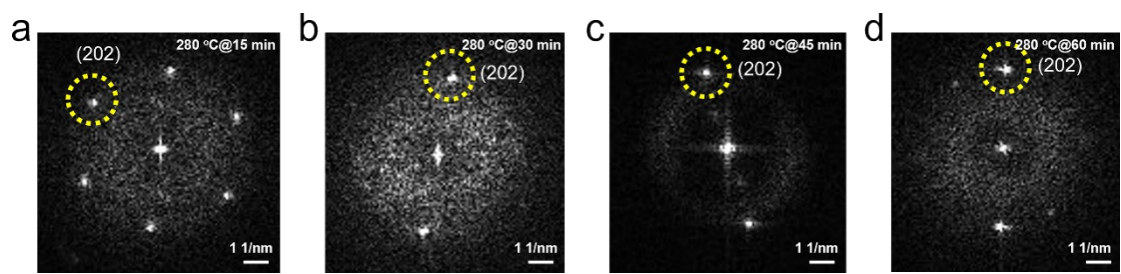


Fig. S9 The FFT images shown correspond to the RHTEM images of CsEuBr₃ NCs synthesized at 280 °C for different reaction time: (a) 15 min; (b) 30 min; (c) 45 min; (d) 60 min.

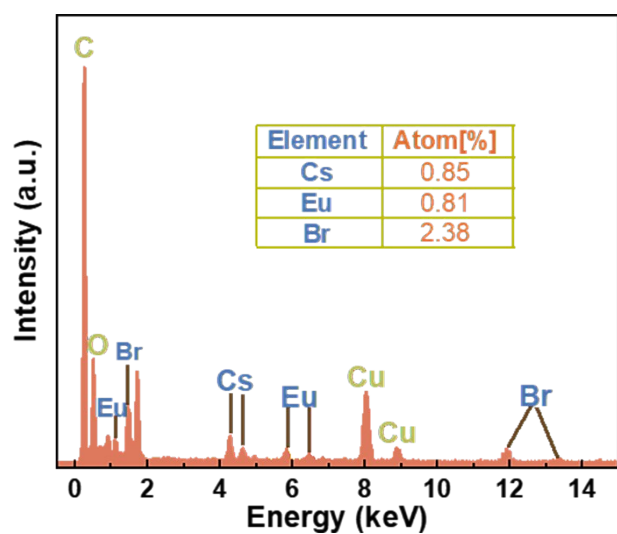


Fig. S10 Energy dispersive spectroscopy (EDS) spectrum and the composition analysis of CsEuBr_3 NCs.

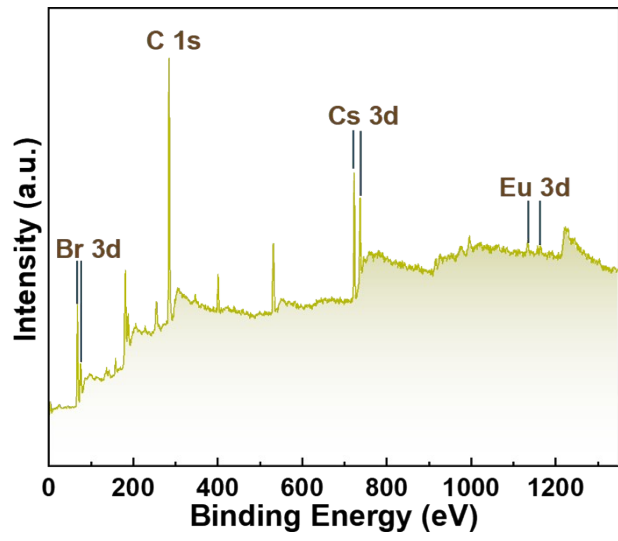


Fig. S11 XPS spectrum of CsEuBr_3 NCs.

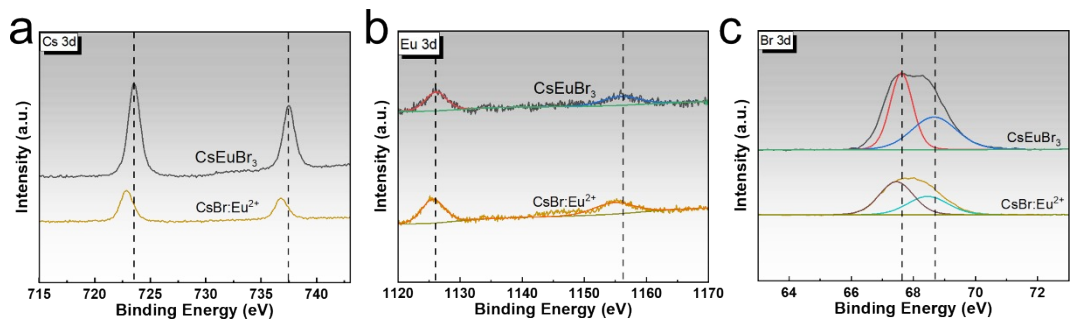


Fig. S12 XPS spectra and the relevant results of different elements: (a) Cs 3d, (b) Eu 3d, (c) Br 3d of CsEuBr₃ NCs, and CsBr:Eu²⁺.

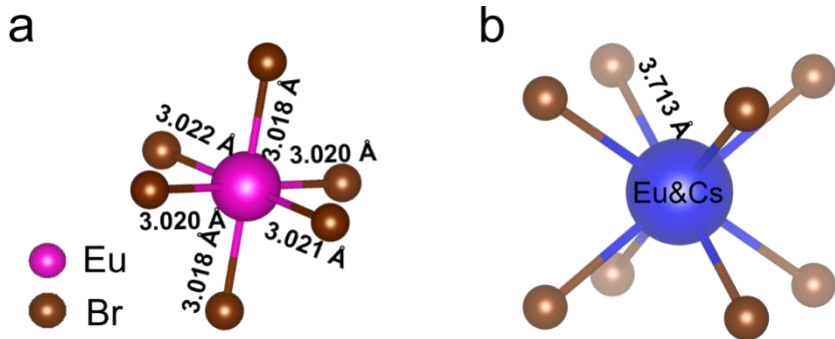


Fig. S13 (a) $[\text{EuBr}_6]^{4-}$ cluster octahedral structure. (b) $[(\text{Eu}\&\text{Cs})\text{Br}_8]^{6-}$ cluster cubic structure.

To distinguish the red-shift of the emission peaks of CsEuBr_3 NCs compared to $\text{CsBr}:\text{Eu}^{2+}$ NCs, we introduce a distorted lattice to explain the red shift of the emission spectrum of CsEuBr_3 . The distortion index D can be expressed as,¹

$$D = \frac{1}{n} \sum_{i=1}^n \frac{|d_i - d_{av}|}{d_{av}} \quad \text{** MERGEFORMAT (4)}$$

where n denotes the number of ligands, d_{av} denotes the average distance, and d_i denotes the distance between Eu^{2+} and the i -th ligand Br^- . The distortion index of CsEuBr_3 is calculated as 3.88×10^{-4} , which is greater than the distortion index of $\text{CsBr}:\text{Eu}^{2+}$, resulting in a red shift of the emission peak of CsEuBr_3 NCs.

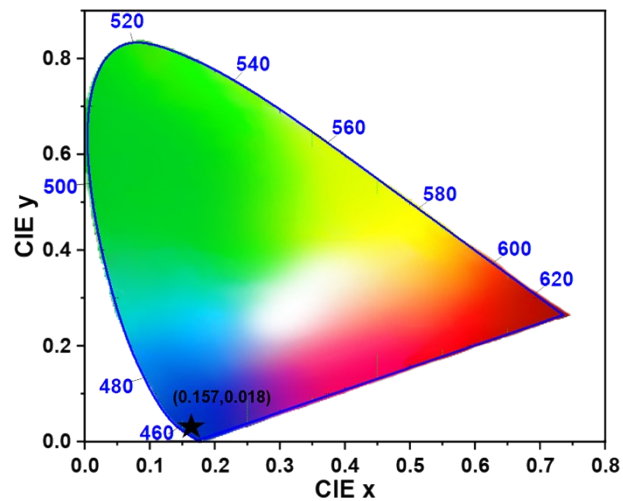


Fig. S14 CsEuBr_3 NCs deep blue emission in CIE coordinates.

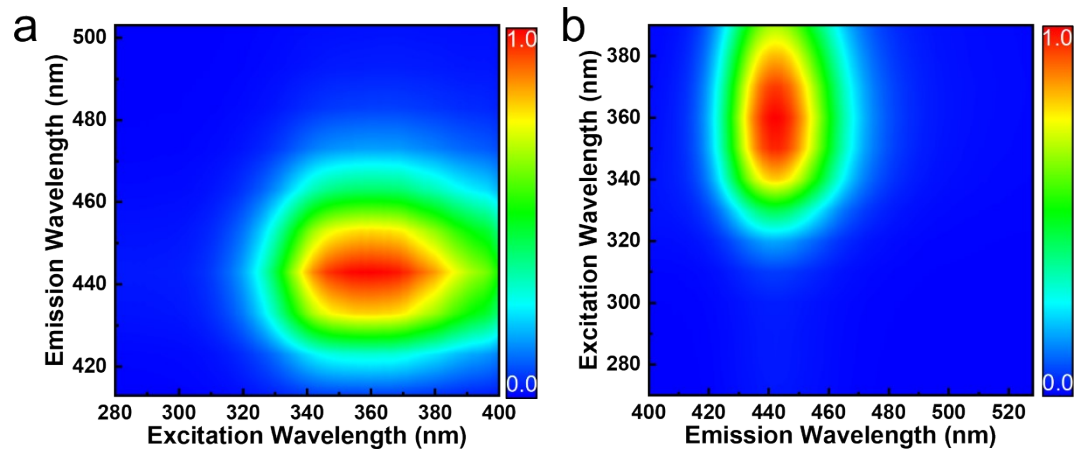


Fig. S15 (a) Detection of emission spectra corresponding to different excitations. (b) Detection of the excitation spectra corresponding to the different emissions.

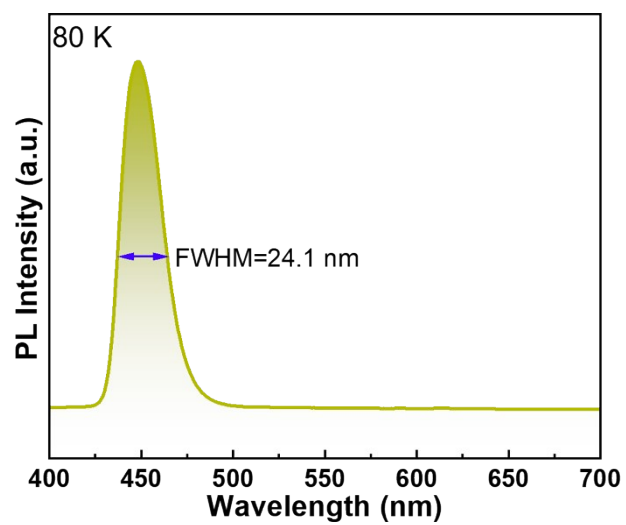


Fig. S16 FWHM of CsEuBr_3 NCs at 80 K.

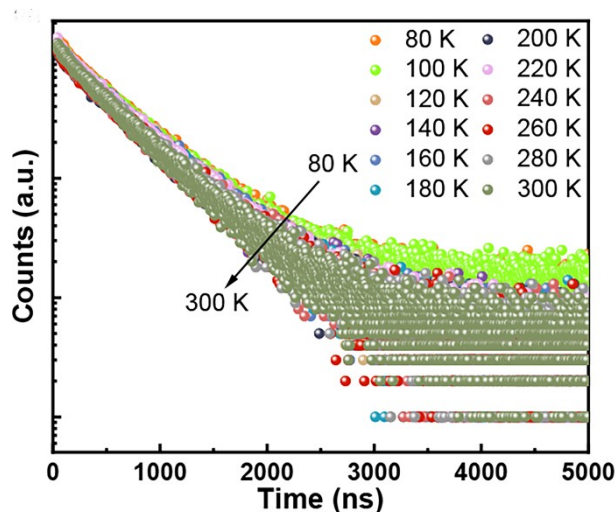


Fig. S17 TRPL decay curves of CsEuBr₃ NCs upon 340 nm excitation monitored at 443 nm from 80 to 300 K.

Fig. S17 shows a typical PL decay curve of CsEuBr₃ NCs monitored at 443 nm emission at 88-300 K. The results indicate that the PL lifetime of CsEuBr₃ at 80 K is longer than that at 300 K, which may be related to the thermally assisted escape route and temperature-dependent rapid non-radiative recombination.

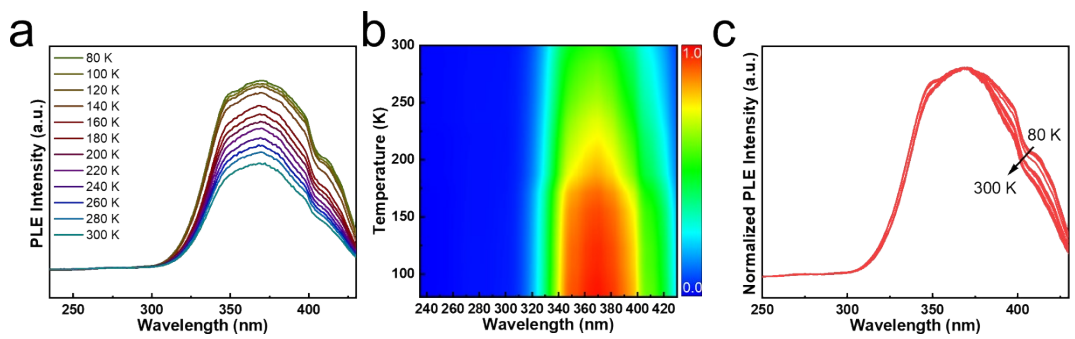


Fig. S18 (a) Temperature-dependent PLE spectra of CsEuBr_3 NCs. (b) Pseudocolor map of temperature-dependent PLE spectra of the CsEuBr_3 NCs. (c) Normalized temperature-dependent PLE spectra of CsEuBr_3 NCs.

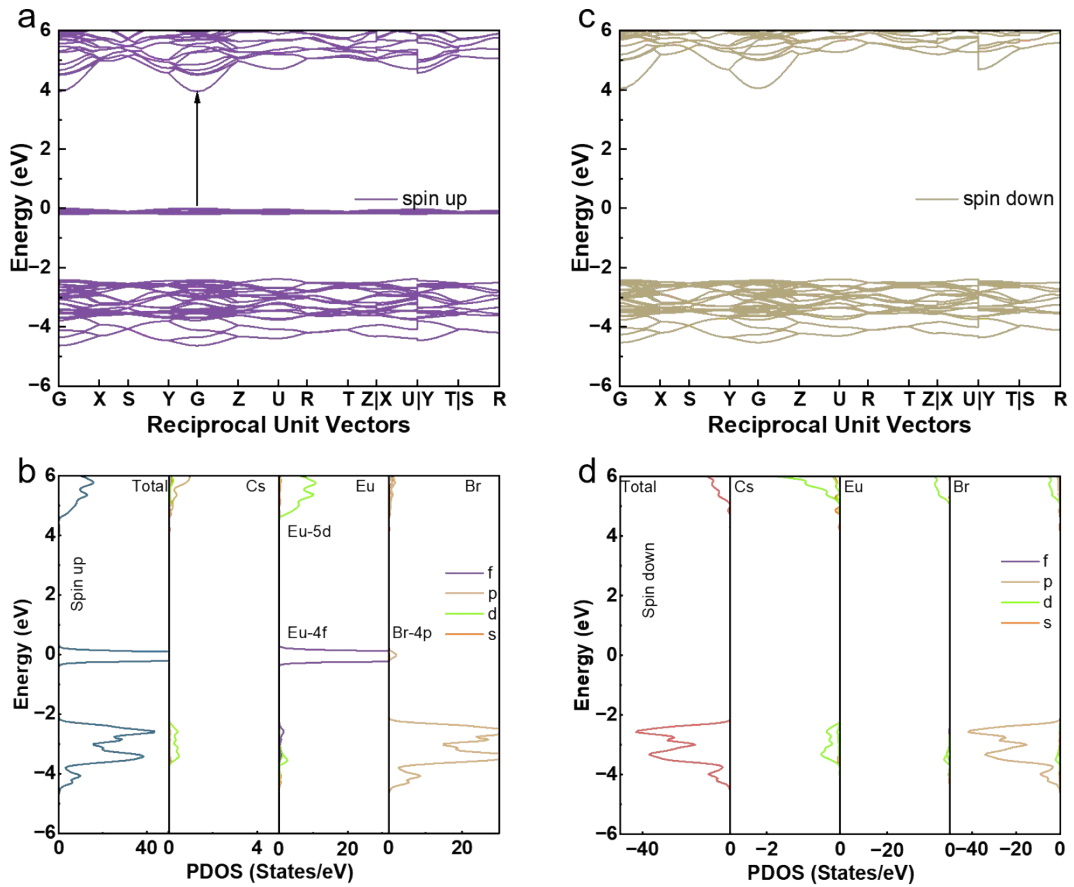


Fig. S19 (a) The band structure and (b) PDOS of CsEuBr_3 hosts calculated with the PEBO functional with spin-up electrons, respectively. (c) The band structure and (d) PDOS of CsEuBr_3 hosts calculated with the PEBO functional with spin-down electrons, respectively.

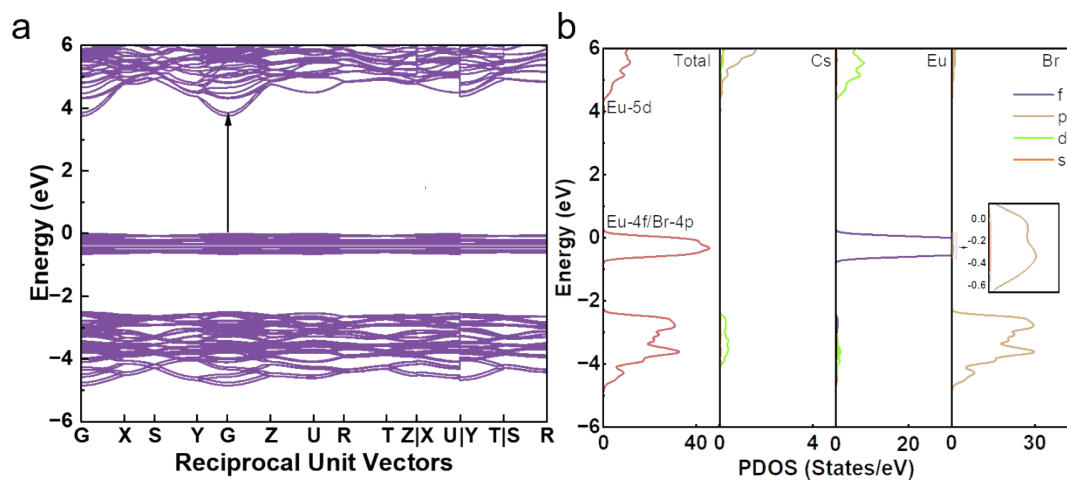


Fig. S20 (a) The band structure and (b) PDOS of CsEuBr₃ hosts calculated with the PBE0+SOC functional, respectively.

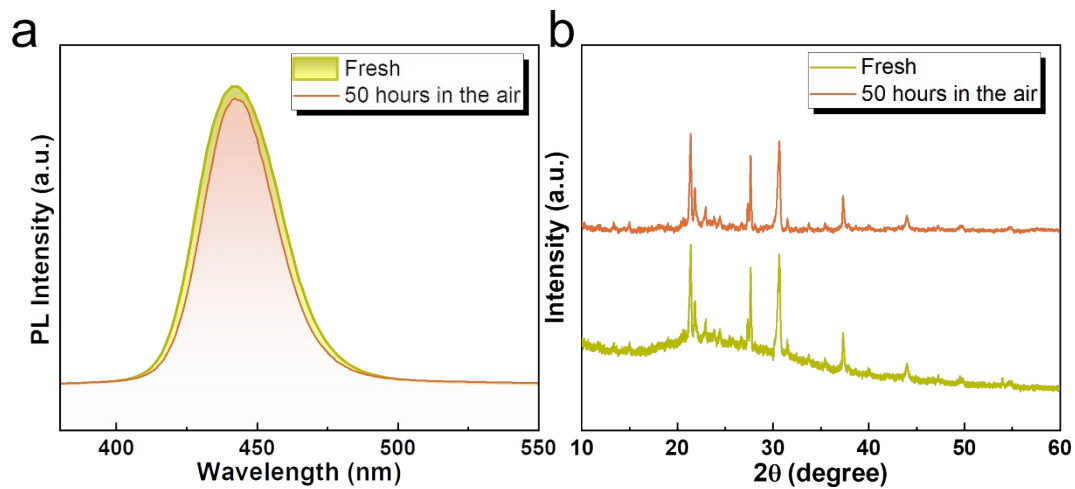


Fig. S21 CsEuBr_3 NCs films placed in an air environment ($25\text{--}30^\circ\text{C}$, $20\text{--}30\%$ humidity)

for 50 h of a) PL and b) XRD.

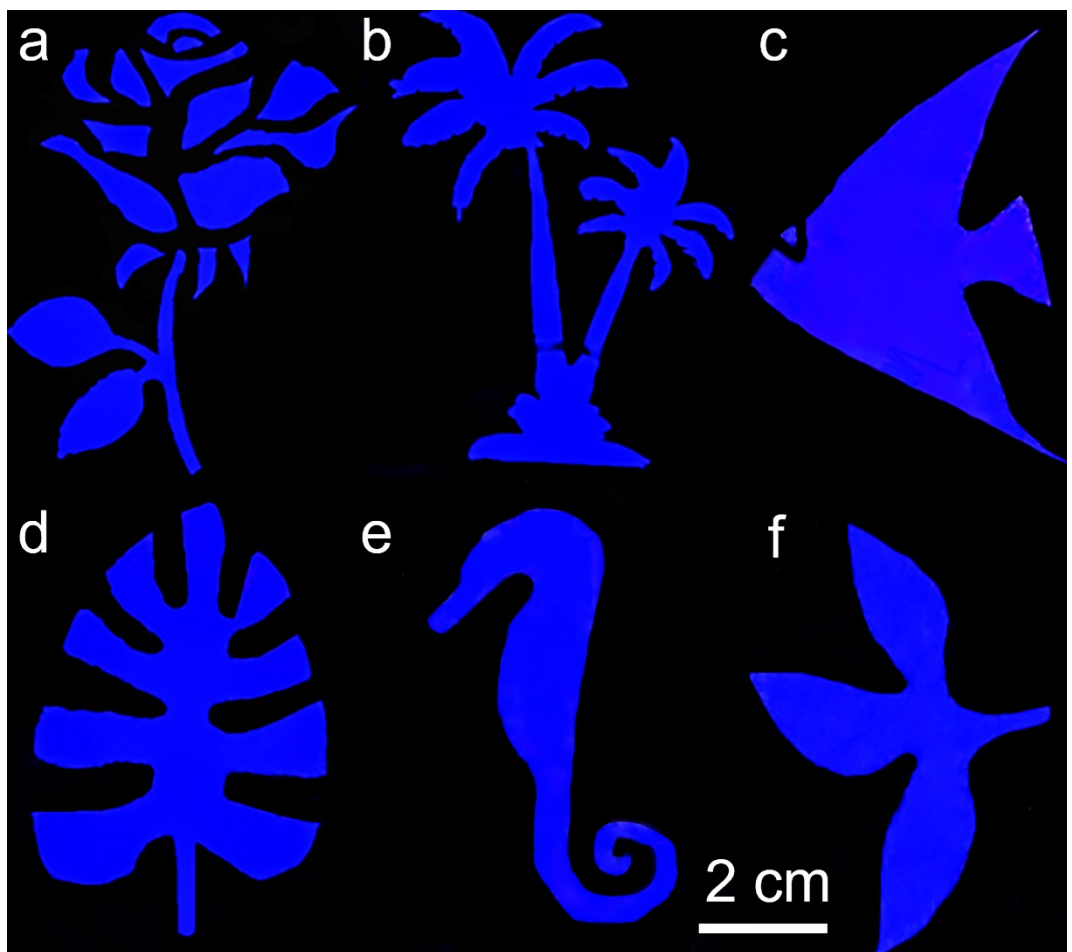


Fig. S22 (a) “Rose”, (b) “coconut tree”, (c) “flounder”, (d) “turtle leaf”, (e) “seahorse”, and (f) “clover” patterns made with composite film ink print.

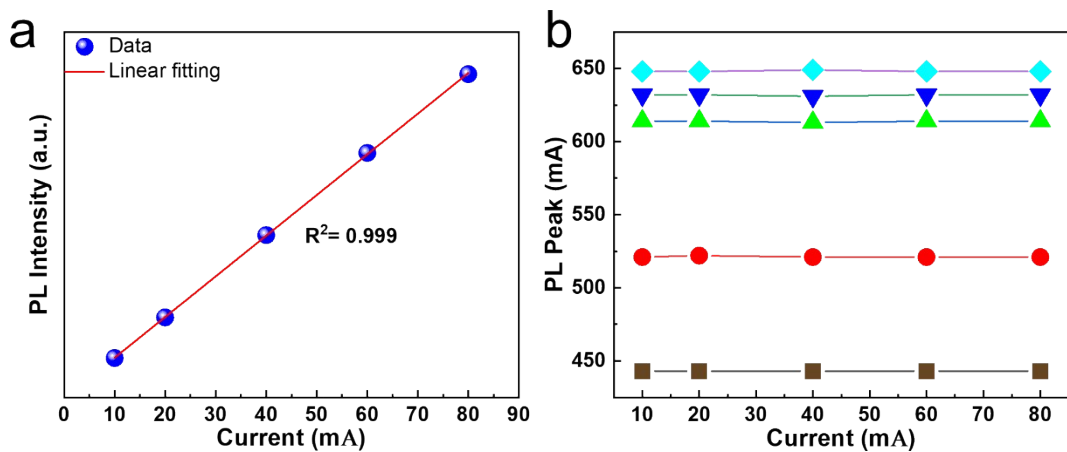


Fig. S23 (a) PL integral intensity and (b) peak luminescence of WLED with different driving currents.

The PL intensity and drive current follow a linear relationship equation:

$$y = ax + b \quad \backslash^* \text{ MERGEFORMAT (6)}$$

x is the drive current, a and b are constants.

Table S1 Summary of different experimental conditions.

Experiment number	Reaction temperature	Reaction time	Eu to Cs molar feed ratio
1	280 °C	45 min	4:1
2	280 °C	45 min	4:2
3	280 °C	45 min	4:3
4	280 °C	45 min	4:4
5	240 °C	45 min	4:1
6	260 °C	45 min	4:1
7	280 °C	45 min	4:1
8	300 °C	45 min	4:1
9	280 °C	15 min	4:1
10	280 °C	30 min	4:1
11	280 °C	45 min	4:1
12	280 °C	60 min	4:1

Table S2 Comparison of the properties of CsEuBr_3 NCs with lead-based perovskites.

Fluorescent materials	Emission peak (nm)	PLQY (%)	exciton lifetime (ns)	Huang-Rhys factor	Ref.
CsPbCl_3 NCs	460	80	–	–	2
CsPbBr_3 NCs	454	70	–	–	3
$\text{CsPb}(\text{Br}_{x}\text{Cl}_{1-x})_3$ NCs	488	82.19	32.9	–	4
CsPbBr_2Cl NCs	475	37.2	13.21	–	5
CsPbBr_3 NCs	459	90	3.84	–	6
$\text{CsPb}(\text{Br}_{x}\text{Cl}_{1-x})_3$ NCs	488	82.19	5.27	–	7
$\text{CsPb}(\text{Br}_{x}\text{Cl}_{1-x})_3$ NCs	488	95	21.08	–	8
CsPbBr_3 NCs	–	–	–	0.38	10
CsPbBr_3 NCs	–	–	–	0.38	11
CsEuBr_3 NCs	443	93.51	455.8	1.54	This work

Table S3 Comparison of the mobility and exciton activation energy of CsEuBr_3 NCs with lead-based perovskites.

Fluorescent materials	hole mobility ($\text{cm}^2 \text{ V}^{-1} \text{ s}^{-1}$)	electron mobility ($\text{cm}^2 \text{ V}^{-1} \text{ s}^{-1}$)	exciton binding energy (meV)	Ref.
$\text{CsPb}(\text{Br}_x/\text{Cl}_{1-x})_3$ NCs	1.06×10^{-9}	1.74×10^{-10}		8
CsPbI_3 NCs	2.03×10^{-2}	1.87×10^{-2}		9
FAPbBr ₃ NCs	8.91×10^{-9}	5.67×10^{-8}		12
CsPbBr_3 NCs	2.43×10^{-3}			13
CsPbI_3 NCs	2.3×10^{-1}	5×10^{-1}		14
CsPbBr_3 NCs			47	15
$\text{CsPb}(\text{Br}_{0.75}\text{Cl}_{0.25})_3$ NCs			50.44	16
FAPbBr ₃ NCs			57.55	17
CsPbBr_3 NCs			43.7	18
CsPbBr_3 NCs			38	19
CsPbBr_3 NCs			40	20
CsPbBr_3 NCs			40	21
CsEuBr_3 NCs	3×10^{-1}	5.0	49.69	This work

In terms of mobility parameters, Luo. et al. calculated the hole and electron mobilities of CsEuBr_3 to be 0.30 and $5.0 \text{ cm}^2 \text{ V}^{-1} \text{ s}^{-1}$,²² higher than those of the currently reported lead-based perovskite NCs. The exciton binding energy of CsEuBr_3 NCs is 49.69 meV, similar to lead-based perovskites NCs. Moderate exciton binding energy creates better conditions for carrier transport and exciton coincidence.

Table S4 The color gamut of WLEDs.

Fluorescent materials	Color gamut (% NTSC in CIE 1931)	Ref.
CsPbX ₃	103	23
A ₂ NaScF ₆ (A = K, Rb, Cs):Mn ⁴⁺	108.4	24
CsPbBr ₃ :Sr/PbBr(OH)/molecular	124	25
CsPbX ₃ @glass	127	26
Cs ₃ MnBr ₅	104	27
Cs ₄ PbBr ₆	121.3	28
CsPb(Br/I) ₃	126	29
h-BN@(PMA) ₂ MA _{n-1} PbnBr _{3n+1}	106.1	30
CsEuBr ₃ NCs	127.1	This work

Notes and references

- 1 M. Liao, F. Wu, J. Wang, D. Zhu, X. Zhang, H. Dong, Z. Lin, M. Wen and Z. Mu, *ACS Appl. Mater. Interfaces*, 2022, **14**, 47892
- 2 B.-B. Zhang, S. Yuan, J.-P. Ma, Y. Zhou, J. Hou, X. Chen, W. Zheng, H. Shen, X.-C. Wang, B. Sun, O. M. Bakr, L.-S. Liao and H.-T. Sun, *J. Am. Chem. Soc.*, 2019, **141**, 15423.
- 3 Y. S. Shin, Y. J. Yoon, K. T. Lee, J. Jeong, S. Y. Park, G.-H. Kim and J. Y. Kim, *ACS Appl. Mater. Interfaces*, 2019, **11**, 23401.
- 4 S. Zhang, H. Liu, X. Li and S. Wang, *Nano Energy*, 2020, **77**, 105302.
- 5 W. H. Jeong, Z. Yu, L. Gregori, J. Yang, S. R. Ha, J. W. Jang, H. Song, J. H. Park, E. D. Jung, M. H. Song, S. H. Park, H. J. Snaith, A. Boretti, F. De Angelis, D. Meggiolaro, J. Lee, H. Choi and B. R. Lee, *J. Mater. Chem. A*, 2021, **9**, 26750.
- 6 Y. Xie, B. Peng, I. Bravić, Y. Yu, Y. Dong, R. Liang, Q. Ou, B. Monserrat and S. Zhang, *Adv. Sci.*, 2020, **7**, 2001698.
- 7 G. H. Ahmed, J. K. El-Demellawi, J. Yin, J. Pan, D. B. Velusamy, M. N. Hedhili, E. Alarousu, O. M. Bakr, H. N. Alshareef and O. F. Mohammed, *ACS Energy Lett.*, 2018, **3**, 2301.
- 8 H. Zhu, G. Tong, J. Li, E. Xu, X. Tao, Y. Sheng, J. Tang and Y. Jiang, *Adv. Mater.*, 2022, **34**, 2205092.
- 9 F. Zhao, H. Duan, S. Li, J. Pan, W. Shen, S. Li, Q. Zhang, Y. Wang and L. Liao, *Angew. Chem. Int. Ed.*, 2023, **62**, e202311089.
- 10 Lao. X, Yang. Z, Su. Z, Bao. Y, Zhang. J, Wang. X, Cui. X, Wang. M, Yao. X and Xu. S *J. Phys. Chem. C*, 2019, **123**, 5128.
- 11 C. M. Iaru, J. J. Geuchies, P. M. Koenraad, D. Vanmaekelbergh and A. Y. Silov, *ACS Nano*, 2017, **11**, 11024.
- 12 H. Chen, L. Fan, R. Zhang, C. Bao, H. Zhao, W. Xiang, W. Liu, G. Niu, R. Guo, L. Zhang and L. Wang, *Adv. Opt. Mater.*, 2020, **8**, 1901390.
- 13 Y. Gao, Y. Liu, F. Zhang, X. Bao, Z. Xu, X. Bai, M. Lu, Y. Wu, Z. Wu, Y. Zhang, Q. Wang, X. Gao, Y. Wang, Z. Shi, J. Hu, W. W. Yu and Y. Zhang, *Adv. Mater.*, 2022, **34**, 2207445.
- 14 E. M. Sanehira, A. R. Marshall, J. A. Christians, S. P. Harvey, P. N. Ciesielski, L. M. Wheeler, P. Schulz, L. Y. Lin, M. C. Beard and J. M. Luther, *Sci. Adv.*, 2017, **3**, eaao4204.
- 15 B. T. Diroll, H. Zhou and R. D. Schaller, *Adv. Funct. Mater.*, 2018, **28**, 1800945.
- 16 H. M. Ghaithan, S. M. H. Qaid, Z. A. Alahmed, M. Hezam, A. Lyras, M. Amer and A. S. Aldwayyan, *J. Phys. Chem. C*, 2021, **125**, 886.

- 17 D. Han, M. Imran, M. Zhang, S. Chang, X. Wu, X. Zhang, J. Tang, M. Wang, S. Ali, X. Li, G. Yu, J. Han, L. Wang, B. Zou and H. Zhong, *ACS Nano*, 2018, **12**, 8808.
- 18 Z. Shi, Y. Li, Y. Zhang, Y. Chen, X. Li, D. Wu, T. Xu, C. Shan and G. Du, *Nano Lett.*, 2017, **17**, 313.
- 19 Q. Zhang, R. Su, X. Liu, J. Xing, T. C. Sum and Q. Xiong, *Adv. Funct. Mater.*, 2016, **26**, 6238.
- 20 X. Li, Y. Wu, S. Zhang, B. Cai, Y. Gu, J. Song and H. Zeng, *Adv. Funct. Mater.*, 2016, **26**, 2435.
- 21 B. Ai, C. Liu, Z. Deng, J. Wang, J. Han and X. Zhao, *Phys. Chem. Chem. Phys.*, 2017, **19**, 17349.
- 22 J. Luo, L. Yang, Z. Tan, W. Xie, Q. Sun, J. Li, P. Du, Q. Xiao, L. Wang, X. Zhao, G. Niu, L. Gao, S. Jin and J. Tang, *Adv. Mater.*, 2021, **33**, 2101903.
- 23 J. Lin, Y. Lu, X. Li, F. Huang, C. Yang, M. Liu, N. Jiang and D. Chen, *ACS Energy Lett.*, 2021, **6**, 519.
- 24 Y. Y. Zhou, E. H. Song, M. G. Brik, Y. J. Wang, T. Hu, Z. G. Xia and Q. Y. Zhang, *J. Mater. Chem. C*, 2019, **7**, 9203.
- 25 T. Xuan, S. Guo, W. Bai, T. Zhou, L. Wang, R.-J. Xie, *Nano Energy*, 2022, **95**, 107003.
- 26 S. Chen, J. Lin, S. Zheng, Y. Zheng and D. Chen, *Adv. Funct. Mater.*, 2023, **33**, 2213442.
- 27 B. Su, M. S. Molokeev and Z. Xia, *J. Mater. Chem. C*, 2019, **7**, 11220.
- 28 X. Chen, F. Zhang, Y. Ge, L. Shi, S. Huang, J. Tang, Z. Lv, L. Zhang, B. Zou and H. Zhong, *Adv. Funct. Mater.*, 2018, **28**, 1706567.
- 29 Q. Wang, Y. Tong, M. Yang, H. Ye, X. Liang, X. Wang and W. Xiang, *J. Mater. Sci. Technol.*, 2022, **121**, 140.
- 30 G. Zhou, Y. Xu and Z. Xia, *ACS Appl. Mater. Interfaces*, 2020, **12**, 27386.